Aberration characterization for the optimal design of high-resolution endoscopic optical coherence tomography catheters

Wladimir A. Benalcazar,[1,2] Woonggyu Jung,[2,4] and Stephen A. Boppart[1,2,3]

[1]*Department of Electrical and Computer Engineering, University of Illinois at Urbana-Champaign, Urbana, Illinois 61801, USA*

[2]*Beckman Institute for Advanced Science and Technology, University of Illinois at Urbana-Champaign, Urbana, Illinois 61801, USA*

[3]*Departments of Bioengineering and Internal Medicine, University of Illinois at Urbana-Champaign, Urbana, Illinois 61801, USA*

[4]*Now at the School of Nano-Bioscience and Chemical Engineering,*
Ulsan National Institute of Science and Technology, Ulsan, 689-798, South Korea

*Corresponding author: boppart@illinois.edu

We study the major factors causing degradation in the lateral resolution of gradient-index-lens-based catheters used for high-resolution optical coherence tomography. Chromatic aberration and astigmatism were taken into account in the propagation of broadband single-mode Gaussian beams through the catheter geometry. It was found that, while chromatic aberration did not preclude achieving high resolution, astigmatism posed a major technical difficulty, because its correction requires a very sensitive adjustment of parameters, especially for catheters with long working distances.   © 2012 Optical Society of America

OCIS codes: 180.1655, 120.4820.

Optical coherence tomography (OCT) is an emerging imaging modality that offers noninvasive, real-time cross-sectional images of tissue microanatomy [1]. An important merit of OCT is the possible miniaturization of OCT beam delivery systems with optical fiber and micro-optics [2–4], which has provided easy integration with existing endoscopes and enabled *in vivo* monitoring of luminal organs [5,6]. Since various diseases in internal organs arise in the superficial layers well suited for inspection by OCT, endoscopic OCT has been broadly used to screen suspicious luminal tissues.

Many endoscopic OCT systems have been developed for high-resolution imaging. However, their resolutions in the axial and lateral orientations significantly differ [7,8]. Ultrabroadband optical fields, such as those arising from supercontinuum generation, have succeeded in imaging with submicrometer axial resolutions [8]. However, lateral resolutions in endoscopic OCT are typically above 20 μm. Despite this, relatively few studies have been reported that describe the enhancement of the lateral resolution [9–11]. In this study, we characterize the aberrations responsible for the degradation of the lateral resolution in gradient-index (GRIN)-lens-based catheters.

Consider a forward imaging probe consisting of a single-mode fiber, a glass rod of length l_r, and a GRIN lens of length $l_g = 2\pi \times \mathrm{pitch}/g$, where g is the gradient constant (Fig. 1). We first simulate the propagation of a broadband, single-mode (TEM_{00}) Gaussian beam along the optical components of such catheter. In the paraxial approximation, the beam emerging from a fiber oriented along direction z and having wavelength λ (wave vector $k = 2\pi n/\lambda$) and mode field radius W_0 has a field

$$\Psi(r,z) = i\psi(r,z)e^{-ikz}, \quad \text{with} \quad \psi(r,z) = iz_0/q(z)e^{-i\frac{kr^2}{2q(z)}}.$$

Here $z_0 = (\pi W_0^2)/\lambda$ is the confocal parameter and $r = \sqrt{x^2 + y^2}$ is the radial coordinate. This field can be uniquely characterized by the complex parameter

$q(z) = z + iz_0$, where z is the distance to focus. The propagation through components characterized by the so-called ABCD matrix was carried out by the operation $q' = (\mathrm{A}q + \mathrm{B})/(\mathrm{C}q + \mathrm{D})$. Our calculations used a fiber with refractive indices of 1.461 for the core and 1.456 for the cladding, and a core radius of 1.7 μm (SM600, Thorlabs, Newton, New Jersey), a glass rod of BK7 material, and a commercially available GRIN lens with a gradient constant g of 660 m^{-1} and a diameter of 1 mm.

To account for chromatic effects, the spectrum of the field was considered within 2 standard deviations (spanning 200 nm) apart from the center wavelength λ_0 of 800 nm in a Gaussian spectrum of 120 nm of bandwidth (FWHM), and the propagation was performed taking into account the dispersive refractive indices of all the optical components comprising the catheter.

Because of the chromatic aberration, augmenting the bandwidth to improve axial resolution comes at the expense of increasing the lateral spot size Δ_r (i.e., the lateral resolution, which is measured as the diameter of the circle of least confusion of the beam over the considered wavelength range), as seen in Fig. 2(a). Given a fixed bandwidth, the chromatic lateral broadening of the spot size is particularly notorious for high-resolution probes, as seen in Fig. 2(b). While the spot size at the center
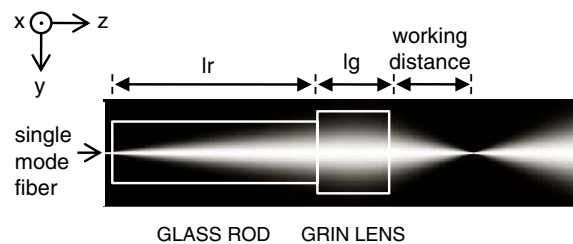

Fig. 1. Schematic of a forward-directed probe and its main components: glass rod and GRIN lens. All simulations in this article assume the presence of tissue beyond the catheter.

© 2012 Optical Society of America

wavelength goes below 2 μm, the broadband spot size does not. The observed result is the consequence of the propagation through long rods required to achieve high lateral resolutions. On one hand, the long propagation through the rod expands the beam to fill the aperture of the lens for high resolution, but, on the other hand, this long propagation enhances the chromatic aberration. The first factor reduces the spot size, but for high enough resolutions, the second factor becomes significant and the spot size increases.

The length of the glass rod and the GRIN lens determine both the working distance and the lateral resolution. Contour plots for working distances and resolutions are shown in the chart of Fig. 2(c). There is a useful zone for probe design in between the two jagged lines, each of which corresponds to a probe focusing at infinity (left) and at zero working distance (right). To the left of this zone, probes are unfeasible, as the beams diverge. To its right, probes focus inside the GRIN lens. Given a fixed working distance [black curves in Fig. 2(c)], the resolution can be chosen within a range, or vice versa. This gives the flexibility to adjust both the resolution and the depth of field required for a given application. As seen before, minimizing the lateral resolution requires the use of long rods that expand the beam enough to fill the GRIN lens, so as to increase the numeric aperture of the probe at its focusing side. For example, for probes with no rods, resolutions no better than 12.1, 8.5, and 7.3 μm at respective working distances of 2, 1, and 0.5 mm can be obtained. On the other hand, with rods of length of 6.3 mm (which would expand the beam enough to fill 80% of the width of the 1 mm diameter GRIN lens), resolutions of 4.1, 2.8, and 2.1 μm are achievable. Going beyond that rod length is useless, as chromatic aberration worsens the lateral resolution. Thus, the limit in lateral resolution is set by the numeric aperture of the GRIN lens and chromatic aberration, which are determined by the lens radius of the

catheter and the beam bandwidth, respectively. For the lens of 1 mm in diameter and the bandwidth considered here, neither of these factors impedes the construction of catheters with high lateral resolutions. However, for smaller diameter lenses (e.g., 500 μm in diameter), the numeric aperture severely limits the resolution [see red lines in Fig. 2(c)]. An alternative way to mitigate the degradation in the resolution is to use GRIN lenses with higher gradient constants, as they will reduce the lens thickness while increasing the numeric aperture of the catheter.

The model was used beyond the configuration of Fig. 1 to study radial imaging probes, in which the cylindrical symmetry of the beam is lost due to the cylindrical window at the catheter sheath through which the beam is sent into the sample [Fig. 3(a)]. For this case, the optical field can be written as $\Psi(x, y, z) = i\psi_x(x,z)\psi_y(y,z)e^{ikz}$, which can be uniquely characterized by the beam parameters $q_x(z_x) = z_x + iz_{0x}$ and $q_y(z_y) = z_y + iz_{0y}$.

Consider the design of a catheter for radial imaging at a working distance z_y into the sample (where y represents the azimuthal orientation). To this end, a BK7 prism and a polyestyrene sheath are added to the design in Fig. 1. The sheath has a cylindrical window with an inner radius R_1 of 750 μm, an outer radius R_2 of 1000 μm, and refractive index n_t, and serves to preserve the structural integrity of the catheter by isolating it from the exterior. The prism, which has a side dimension of 700 μm, deflects the beam by 90° toward the sheath window [Fig. 3(a)]. Although this is the most common configuration, it has an air

Fig. 3. (Color online) Correction of astigmatism in OCT probes. (a) Schematic of beam waist along both the longitudinal (x) and azimuthal (y) orientations. (b) Azimuthal resolution Δ_y (green) and astigmatic ratio Δ_x/Δ_y (blue) as functions of rod length and lens pitch before matching refractive index (both Δ_x and Δ_y are measured at a distance z_y from the catheter). The horizontal line indicates the rod length used for (c) and (d), which corresponds to a maximum beam radius of 375 μm inside the GRIN lens. (c) Azimuthal resolution (green) and resolution astigmatic ratio (blue) and (d) azimuthal working distance z_y (green) and working distance astigmatic ratio z_x/z_y (blue) as functions of matching refractive index n_c and pitch. The red curve corresponds to parameters that fully suppress astigmatism.
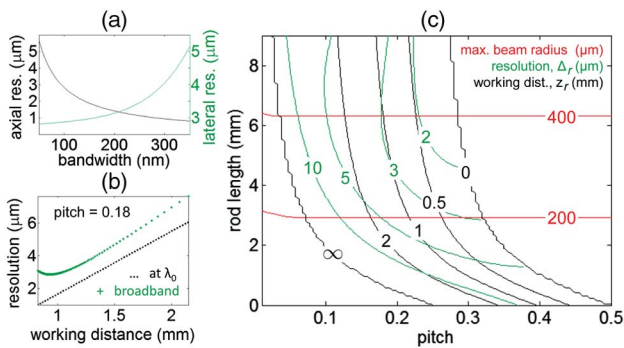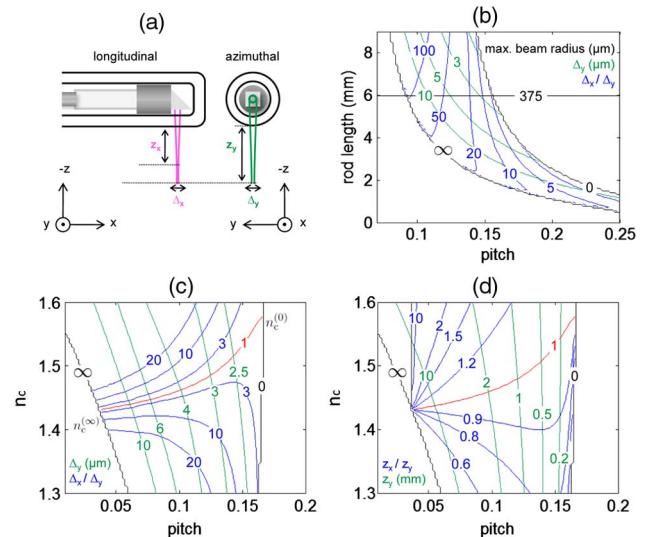
Fig. 2. (Color online) Chromatic aberration in OCT catheters. (a) Axial and lateral resolutions for OCT as a function of the spectral bandwidth. (b) Broadband lateral resolution (green crosses) and lateral resolution at center wavelength λ_0 (black dots) versus working distance (the working distance is varied by changing the length of the glass rod from 2 to 9 mm at a fixed pitch of 0.18). (c) Probe design chart showing the values of the broadband lateral resolution Δ_r (green) and working distance z_r (black) as functions of the parameters rod length l_r and GRIN lens pitch. Red lines indicate the maximum beam radius inside the GRIN lens. All calculations use $\lambda_0 = 800$ nm. (b) and (c) use a bandwidth of 120 nm (FWHM).

gap between the flat face of the prism and the cylindrical surface of the sheath, which introduces astigmatism in the beam (the inner surface of the window acts as a divergent lens in the azimuthal orientation y). The effect of astigmatism, measured as the ratio of the longitudinal resolution over the azimuthal resolution, is shown in Fig. 3(b). Notice that, even when a rod of length 6 mm is used to fill in ~80% of the aperture of the GRIN lens, the ratio is as high as 5 for small spot sizes and working distances, and increases for larger spot sizes and corresponding working distances up to 100.

To correct this aberration, previous approaches have used cylindrical lenses [9] and mirrors [10]. Here, we simulate the effect of adding a refractive index matching medium with refractive index n_c to fill in the air gap between the prism and the inner surface of the sheath, because such an approach is more mechanically stable and less costly. Currently, matching refractive indices can be achieved by a variety of products that mimic fused silica, BK7, acrylic, and others. Figures 3(c) and 3(d) show the azimuthal resolutions Δ_y and working distances z_y, as well as the astigmatic ratios Δ_x/Δ_y and z_x/z_y as functions of n_c and GRIN lens pitch for a rod length of 6 mm. Note that, by comparing the astigmatic ratios along the straight black line in Fig. 3(b) and those achieved in Fig. 3(c), astigmatism is significantly reduced by the use of the matching medium. In particular, there is an ideal line in the parameter space in which both the working distances and resolutions are the same in both orientations (red line), but is accessible only within a range of matching refractive indexes $n_c^{(0)} \le n_c \le n_c^{(\infty)}$, where $n_c^{(0)} = n_t$ and

$$n_c^{(\infty)} = n_t \left[1 + \frac{R_1}{R_2} \left(1 - \frac{n_t}{n_s} \right) \right]^{-1}$$

are the limiting cases that correspond to matching refractive indices for catheters focusing at 0 and ∞ working distances, respectively. Note that total correction of astigmatism is possible at any working distance, provided that the matching refractive index is precisely chosen, and that this refractive index becomes more sensitive to the ratio R_1/R_2 for long working distances. In practice, high precision in the refractive index of the medium may not be achievable. Instead, for an available refractive index n_c, the rod length can be adjusted to choose the desired azimuthal working distance.

The performance of the catheter is very sensitive to variations of the parameters. A robust design is more difficult to achieve for long-working-distance catheters, because small changes in the refractive index of the sample (e.g., when going from stromal to fat-rich regions during scanning) could distort the azimuthal resolutions and working distances above the values needed for high-resolution OCT, while for short-working-distance high-resolution probes, matching the sheath refractive index suffices. The lack of robustness in the correction of astigmatism poses the most difficult limit to overcome in probe design. On the other hand, limitations in the lateral resolution due to chromatic aberration do not preclude achieving sufficient resolution for high-resolution imaging with catheters of 1 mm in diameter or more, and a careful combination of lens pitch and length of a glass rod allows for customizing both working distance and lateral resolution within a range of parameters suitable for many endoscopic OCT applications, as well as for possible integration of OCT with other nonlinear optical imaging modalities.

References

1. D. Huang, E. Swanson, C. Lin, J. Schuman, W. Stinson, W. Chang, M. Hee, T. Flotte, K. Gregory, C. Puliafito, and J. G. Fujimoto, Science **254**, 1178 (1991).
2. G. J. Tearney, S. A. Boppart, B. E. Bouma, M. E. Brezinski, N. J. Weissman, J. F. Southern, and J. G. Fujimoto, Opt. Lett. **21**, 543 (1996).
3. G. J. Tearney, M. E. Brezinski, B. E. Bouma, S. A. Boppart, C. Pitris, J. F. Southern, and J. G. Fujimoto, Science **276**, 2037 (1997).
4. Z. Yaqoob, J. Wu, E. J. McDowell, X. Heng, and C. Yang, J. Biomed. Opt. **11**, 063001 (2006).
5. I.-K. Jang, G. J. Tearney, B. MacNeill, M. Takano, F. Moselewski, N. Iftima, M. Shishkov, S. Houser, H. T. Aretz, E. F. Halpern, and B. E. Bouma, Circulation **111**, 1551 (2005).
6. J. G. Fujimoto, S. A. Boppart, G. J. Tearney, B. E. Bouma, C. Pitris, and M. E. Brezinski, Heart **82**, 128 (1999).
7. B. E. Bouma, G. J. Tearney, C. C. Compton, and N. S. Nishioka, Gastrointest. Endosc. **51**, 467 (2000).
8. Y. Chen, P. M. Andrews, A. D. Aguirre, J. M. Schmitt, and J. G. Fujimoto, J. Biomed. Opt. **12**, 034008 (2007).
9. P. Meemon, K.-S. Lee, S. Murali, and J. Rolland, Appl. Opt. **47**, 2452 (2008).
10. J. Xi, L. Huo, Y. Wu, M. J. Cobb, J. H. Hwang, and X. Li, Opt. Lett. **34**, 1943 (2009).
11. A. R. Tumlinson, B. Považay, L. P. Hariri, J. McNally, A. Unterhuber, B. Hermann, H. Sattmann, W. Drexler, and J. K. Barton, J. Biomed. Opt. **11**, 064003 (2006).